Title

PROBING NEARBY COSMIC-RAY ACCELERATORS AND INTERSTELLAR MEDIUM TURBULENCE WITH MILAGRO HOT SPOTS

Journal

The Astrophysical Journal, 721(1)

ISSN

0004-637X

Authors

Malkov, MA
Diamond, PH
Drury, L O'C
et al.

Publication Date

2010-09-20

DOI

10.1088/0004-637x/721/1/750

Peer reviewed

The Astrophysical Journal, 721:750–761, 2010 September 20 doi:10.1088/0004-637X/721/1/750

PROBING NEARBY COSMIC-RAY ACCELERATORS AND INTERSTELLAR MEDIUM TURBULENCE WITH MILAGRO HOT SPOTS

M. A. Malkov[1], P. H. Diamond[1], L. O'C. Drury[2], and R. Z. Sagdeev[3]
[1] CASS and Department of Physics, University of California, San Diego, La Jolla, CA 92093-0424, USA
[2] Dublin Institute for Advanced Studies, 31 Fitzwilliam Place, Dublin 2, Ireland
[3] University of Maryland, College Park, MD 20742-3280, USA
Received 2010 May 7; accepted 2010 July 28; published 2010 September 1

ABSTRACT

Both the acceleration of cosmic rays (CRs) in supernova remnant shocks and their subsequent propagation through the random magnetic field of the Galaxy are deemed to result in an almost isotropic CR spectrum. However, the MILAGRO TeV observatory discovered sharp ($\sim 10^\circ$) arrival anisotropies of CR nuclei. We suggest a mechanism for producing a weak and narrow CR beam which operates en route to the observer. The key assumption is that CRs are scattered by a strongly anisotropic Alfvén wave spectrum formed by the turbulent cascade across the local field direction. The strongest pitch-angle scattering occurs for particles moving almost precisely along the field line. Partly because this direction is also the direction of the minimum of the large-scale CR angular distribution, the enhanced scattering results in a weak but narrow particle excess. The width, the fractional excess, and the maximum momentum of the beam are calculated from a systematic transport theory depending on a single scale l which can be associated with the longest Alfvén wave, which efficiently scatters the beam. The best match to all three characteristics of the beam is achieved at $l \sim 1$ pc. The distance to a possible source of the beam is estimated to be within a few 100 pc. Possible approaches to the determination of the scale l from the characteristics of the source are discussed. Alternative scenarios of drawing the beam from the galactic CR background are considered. The beam-related large-scale anisotropic CR component is found to be energy independent, which is also consistent with the observations.

Key words: acceleration of particles – cosmic rays – diffusion – ISM: supernova remnants – magnetohydrodynamics (MHD) – scattering – shock waves – turbulence

1. INTRODUCTION

The MILAGRO TeV observatory recently discovered collimated beams dominated by hadronic cosmic rays (CRs) with a narrow ($\sim 10^\circ$) angular distribution in the 10 TeV energy range (Abdo et al. 2008). This is surprising since most of the CR acceleration and propagation models predict only a weak, large-scale anisotropy. The acceleration models are based on the diffusive shock acceleration (DSA) mechanism, widely believed to generate galactic CRs in supernova remnant (SNR) shocks. The cornerstone of the DSA is a rapid pitch-angle scattering of CRs by self-generated Alfvén waves in the shock vicinity. An enhanced scattering isotropizes particle distributions. Moreover, when the shock releases the accelerated particles into the interstellar medium (ISM), the ISM turbulence continues to scatter them. Even though this scattering occurs at a significantly lower rate, all sharp anisotropies carried over from the accelerator or created otherwise should be erased during the long ($\gtrsim$100 pc) travel of the CRs from any hypothetical nearby SNR to the observer, yet the astounding sharp beaming effect is argued to be genuine.

Focusing instead on relatively distant accelerators (such as nearby SNRs) and long-distance propagation effects as a possible cause of the MILAGRO beam(s), we do not consider "local" scenarios that have already been discussed and largely rejected by Drury & Aharonian (2008) and Salvati & Sacco (2008). As for the remote accelerator with subsequent propagation effects, some of them have also been suggested in the above publications. In particular, Salvati & Sacco (2008) associate the observed CR beam with the Geminga pulsar. However, Drury & Aharonian (2008) argue that this does not explain the sharp collimation, and suggest a magnetic nozzle as such a collimation device. The magnetic nozzle scenario, however, poses a rather strong constraint on the nozzle mirror ratio ($B_{\max}/B_{\min} \sim \vartheta^{-2} \gg 1$, where ϑ is the beam angular width). The advantage of this scenario is that the beam density is equal to the difference between the isotropic components of CRs on each side of the mirror (by linearity of the transport equation). Since the MILAGRO beam is very weak ($\sim 10^{-4}$ of the CR density), this is a very mild requirement on the CR enhancement on the far side of the mirror. It is also true that the existence of a magnetic mirror of that strength cannot be warranted or denied on any rational grounds. It should be noted that any anisotropic distribution may become vulnerable to self-spreading in pitch angle. As pointed out by Drury & Aharonian (2008), however, the isotropic CR background should produce a stabilizing effect against the beam's self-spreading. We will quantify the CR stabilization in Section 4.4 required for both the collimation mechanism suggested in this paper and for the magnetic nozzle hypothesis.

In this paper, we suggest a novel mechanism for producing a narrow CR beam. It is based on the strong anisotropy of the magnetohydrodynamic (MHD) turbulence in the ISM. Such anisotropy is expected when the turbulence is driven at a long (outer) scale, but unlike the isotropic Kolmogorov cascade, the incompressible MHD cascade is directed perpendicularly to the magnetic field in wave vector space. This was shown by Goldreich & Sridhar (1995, hereafter GS; see also Sridhar & Goldreich 1994 and Goldreich & Sridhar 1997) and confirmed by numerical simulations (e.g., Cho & Vishniac 2000; Maron & Goldreich 2001; Beresnyak & Lazarian 2009). The cascade proceeds to $k_\perp r_g(p) \gg 1$ in the perpendicular wave number direction for the protons with gyroradii $r_g \sim 10^{16}$ cm, typical for the particles of MILAGRO beam energies $pc \sim 10$ TeV and ISM magnetic field of a few μG. As opposed to the $k_\perp$ direction, the spectrum spreading in $k_\parallel$ is

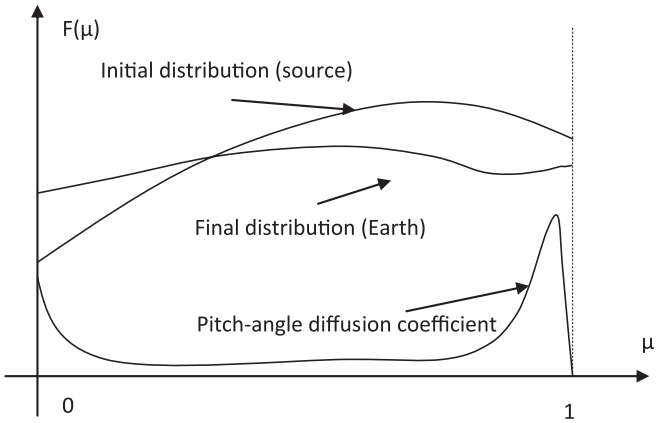

Figure 1. Schematic representation of initial and final pitch-angle distributions and the diffusion coefficient $D_{\mu\mu}(\mu)$.

suppressed, so that $k_\parallel \sim k_\perp^{2/3} l^{-1/3} \ll k_\perp$, where l is the outer scale.

As is known from the wave–particle interaction in plasmas, the scattering of particles with Larmor radii exceeding the wavelength in the perpendicular direction, $k_\perp r_g \gg 1$, is strongly suppressed, since such particles suffer from a rapidly changing electromagnetic force. Specifically, the CR scattering by the GS anisotropic spectrum was investigated in a number of publications (Chandran 2000; Yan & Lazarian 2002). What is important for the purposes of this paper is that the pitch-angle scattering rate is peaked at $|\mu| = |\cos\vartheta| \approx 1$, i.e., for particles moving along the field line, since for these particles $k_\perp r_g(p_\perp) \lesssim 1$. Only particles with such small $p_\perp$, i.e., with pitch angles within $\sin^2\vartheta \lesssim \epsilon \ll 1$ are scattered efficiently. Looking at this problem mathematically, a peaked diffusion coefficient $D(\mu)$ does not necessarily result in a peaked particle distribution $f(\mu)$. Indeed, the time-asymptotic solution of the diffusion equation with zero flux through the boundary is a flat distribution even if the diffusion coefficient is not constant. Nevertheless, consider the particle diffusion in pitch angle on an *intermediate timescale*, i.e., when anisotropy is erased within the strong peak of the diffusion coefficient $D(\mu)$, but is present in the region where $D(\mu)$ is much smaller. The dominant eigenfunction of the scattering operator has a relatively broad minimum at $\mu = 1$, i.e., where D is sharply peaked. Now, the enhanced scattering fills up the very bottom of this minimum, which appears as a narrow excess (Figure 1). In the context of a classical Lorentz gas relaxation problem (Gurevich 1961; Kruskal & Bernstein 1964), this is clearly a transient effect associated with an incomplete decay of the anisotropic part of the pitch-angle distribution. Note that the difference from the Lorenz gas problem is in the sharply peaked $D(\mu)$. In addition, our problem is a problem in z, which is the spatial coordinate (rather than time) along a magnetic flux tube that connects the CR source with Earth.

The demonstration of this phenomenon, facilitated and obscured at the same time by the fact that the peak region $|\sin\vartheta| \ll 1$ contains the singular points of the particle pitch-angle diffusion operator at $\sin\vartheta = 0$, will be the main subject of this paper.

Before we tackle this problem, we briefly discuss in the following section how narrow the CR angular distribution can be as it leaks from a hypothetical nearby SNR accelerator magnetically connected with the heliosphere. This, or some other moderately anisotropic distribution of CRs, created by a recent SNR explosion, will be subjected in Section 3 to the pitch-angle scattering analysis and to the propagation analysis in Section 4. Next, in Section 4.4, we determine the maximum energy of the beam beyond which it must spread on self-generated Alfvén waves. Section 5 deals with the relation between the beam maximum energy and the distance to its possible source. We conclude with a brief discussion of the results and of what the fascinating MILAGRO findings can possibly reveal about a nearby accelerator and the structure of ISM turbulence.

2. ANGULAR DISTRIBUTION OF DIFFUSIVELY ACCELERATED PARTICLES

To estimate the anisotropy of CRs escaping from an SNR accelerator, we first briefly review the DSA mechanism and its possible modifications that can enhance the CR anisotropy. Within this mechanism, particles gain energy by scattering upstream of the shock and back downstream repeatedly. The scattering is supported by strong MHD waves unstably driven by the accelerated particles themselves. In the early phase of acceleration, an ion-cyclotron instability dominates. It is driven by a weak pitch-angle anisotropy of particle distribution. It is reasonable to assume, however, that a small fraction of particles that reach sufficiently high energies can diffuse to the distant part of the turbulent shock precursor where their self-confinement becomes inefficient. In this way, a somewhat artificial notion of the "free escape boundary" (FEB) was introduced, particularly in Monte Carlo numerical schemes (Ellison et al. 1996) and other analytical and numerical studies (Caprioli et al. 2009; Reville et al. 2009). Particle escape also occurs naturally if the plasma upstream is not fully ionized and the weak wave excitation at the periphery of the turbulent shock precursor is suppressed by the ion-neutral collisions (Drury et al. 1996). However, the angular distribution of particles leaking through the FEB has not been calculated systematically. Note that such calculation would require a self-consistent treatment of wave generation and the relaxation of the distribution of leaking particles. If the DSA process inside the precursor maintains CR isotropy, the leaking particles may be assumed to have a one-sided quasi-isotropic distribution.

As the pressure from accelerated particles increases, other instabilities may occur, including the non-resonant fire-hose instability (Achterberg 1983; Shapiro et al. 1998; Bell 2004) and an acoustic instability driven by the *pressure gradient* upstream (Drury & Falle 1986; Zank et al. 1990; Kang et al. 1992). From this point, particle transport becomes more complicated. In particular, acoustic waves turn into shocks and form a shock train that compresses the magnetic field and creates a scattering environment markedly different from the weakly turbulent scattering field described above. It consists of a random sequence of relatively weak shocks and was shown to produce a loss cone in momentum space. However, preliminary calculations of particle dynamics in this environment (Malkov & Diamond 2006) show that the opening angle of runaway particles is still too large to account for the MILAGRO observations, particularly when the subsequent self-spreading of the beam is taken into account. This is clearly necessary since the stabilization on the background CRs is not sufficient at this phase of beam propagation due to its relative strength. Apart from the magnetic nozzle (Drury & Aharonian 2008), a remaining option is to generate the beam on its way to Earth.

At first sight, this task appears to be like "squeezing blood out of stone." Intuitively, an intervening turbulence on the way to

the Earth, if anything, can only further spread the beam. That the turbulent particle beaming is possible nonetheless is primarily due to the very sharp dependence of the scattering frequency on the pitch angle near the magnetic field direction.

3. PITCH-ANGLE SCATTERING OF CRs BY ANISOTROPIC ALFVÉN TURBULENCE

Systematic studies of wave–particle interactions in magnetized plasmas begun in the early 1960s by Sagdeev & Shafranov (1961), Vedenov et al. (1962), and Rowlands et al. (1966), and independently within the astrophysical and geophysical contexts by Jokipii (1966), Kennel & Engelmann (1966), and Völk (1973). The angular profile of the scattering frequency depends on the structure of the turbulence. We provide a concise derivation for the case of our interest in the Appendix. More generally, particle scattering by an anisotropic turbulence with the spectrum suggested by GS was studied by Chandran (2000). Particularly, he demonstrated that the maximum contribution to the pitch-angle scattering of the field-aligned particles is strongly dominated by Alfvén wave magnetic perturbations, and so we neglect the contributions of magnetosonic waves and velocity perturbations in what follows. The neglected components are essential for particles with $|\mu| \ll 1$, but we are primarily interested in those with $\mu \approx 1$, as they are assumed to make one of the MILAGRO "hot spots." Chandran (2000) also gives a detailed description of the pitch-angle diffusion coefficient for the GS spectrum and identifies its peaks at $|\mu| = 0, 1$. However, for the purposes of this paper we need the *angular profile* of the peak at $|\mu| = 1$, which we evaluate in this section.

We begin with the general expression for the pitch-angle scattering coefficient (e.g., Völk 1973; Chandran 2000; see the Appendix):

$$D_{\mu\mu} = \Omega^2(1-\mu^2)\sum_{\mathbf{k},n}\frac{n^2 J_n^2(\xi)}{\xi^2} \times \int_0^\infty I(k_\parallel, k_\perp, \tau) e^{i(k_\parallel v_\parallel + n\Omega)\tau} d\tau, \quad (1)$$

where we have used the (standard) notations provided in the Appendix. Assuming the GS spectrum for the spectral wave density I, we have

$$I = \frac{1}{6\pi} k_\perp^{-10/3} l^{-1/3} g\left(\frac{k_\parallel l^{1/3}}{k_\perp^{2/3}}\right) e^{-\tau/\tau_k}, \quad (2)$$

where we have assumed the notations and normalization of the spectrum used by Chandran (2000) rather than by GS. In particular, $g(x) = H(1-|x|)$, where H is the Heaviside function and $\tau_k = (l/V_A)(k_\perp l)^{-2/3}$ is the turbulence correlation time. Focusing on the resonant interactions with particles, from Equation (1) we obtain

$$D_{\mu\mu} = \frac{\pi}{3} l^{-1/3}\Omega^2(1-\mu^2)\int_0^\infty k_\perp^{-7/3} dk_\perp \sum_{n=-\infty}^{\infty} \times \frac{n^2 J_n^2(\xi)}{\xi^2}\int_{-\infty}^{\infty} g\left(\frac{k_\parallel l^{1/3}}{k_\perp^{2/3}}\right)\delta(k_\parallel v_\parallel - n\Omega) dk_\parallel. \quad (3)$$

Note that the integral in $k_\perp$ cuts off at the lower limit by virtue of the function g. Therefore, from the last expression we can get

$$D_{\mu\mu} = \frac{2\pi}{3}\frac{v}{l|\mu|}(1-\mu^2) y^{4/3} S(y), \quad (4)$$

where we have introduced the notation

$$S(y) = \sum_{n=1}^{\infty} S_n = \sum_{n=1}^{\infty} n^2 \int_{y(n/|\mu|)^{3/2}}^{\infty} J_n^2(x)\, x^{-q} dx, \quad (5)$$

with $y = \sqrt{(1-\mu^2)/\epsilon}$, $\epsilon = v/l\Omega$, and $q = 13/3$. Assuming $y > 1$, we can take an asymptotic limit $x \gg 1$ for J_n and recover the corresponding result of Chandran (2000):

$$D_{\mu\mu} \simeq \frac{2}{13}\zeta\left(\frac{9}{2}\right)\frac{v}{l}\epsilon^{3/2}\frac{|\mu|^{11/2}}{\sqrt{1-\mu^2}}, \quad (6)$$

where $\zeta(s) = \sum_{n=1}^{\infty} n^{-s}$ is the Riemann ζ-function. Note that $\zeta(9/2) \approx 1.05$, so that with a 5% accuracy the $n = 1$ term in Equation (5) would suffice.

For larger values of y, namely, when $\delta \ln(1/\epsilon) \gtrsim \epsilon^{3/2}|\mu|^{11/2}(1-\mu^2)^{-3/2}$, where $\delta = V_A/v \approx V_A/c$, the finite correlation time in the general form of $D_{\mu\mu}$ given by Equations (2) and (3) should be taken into account. It is convenient to perform the integral in $k_\parallel$ first, then perform the one in τ, which yields

$$D_{\mu\mu} = \frac{1}{3} l^{-1/3}\frac{\Omega}{v\mu}(1-\mu^2)\sum_{n=-\infty}^{\infty}\int_{1/l'}^{\infty}\frac{dk_\perp}{k_\perp^{7/3}}\tan^{-1} \times \left\{\frac{1}{\delta}\left[\mu + \frac{n}{\epsilon}(k_\perp l)^{-2/3}\right]\right\}\frac{n^2}{\xi^2} J_n^2(\xi). \quad (7)$$

In contrast to the previous case, the integral here needs to be cut at the lower limit by introducing the longest scale $l' < l$ (Chandran 2000). Perturbations with $k_\perp l' \gtrsim 1$ scatter particles efficiently, while longer waves interact with particles adiabatically. However, to simplify notations we set $l' = l$ below, which is partly justified by a weak dependence of the turbulence intensity on l (Equation (2)). We will discuss our choice of scales l and l' in Section 5.

Expanding $\tan^{-1}$ for a large argument ($\delta, \epsilon \ll 1$) and summing the series of Bessel functions, we obtain

$$D_{\mu\mu} \simeq \frac{\delta\epsilon}{3}\Omega(1-\mu^2)\int_{\epsilon(1-\mu^2)^{1/2}}^{\infty}\frac{d\xi}{\xi}\frac{1-J_0^2(\xi)}{\xi^2} \simeq \frac{1}{6}\frac{v}{l}\delta\left[\ln\left(\frac{1}{\epsilon}\right) - \frac{1}{2}\ln(1-\mu^2)\right](1-\mu^2). \quad (8)$$

Again, within the assumed accuracy, the complete sum with the Bessel functions in Equation (7) yields approximately the same result as only the terms with $n = \pm 1$. We will show below that in calculating the form of the peak of $D_{\mu\mu}(\mu)$ at $|\mu| \approx 1$, it is sufficient to take only the first few terms into account.

Now that we have reviewed the overall behavior of the pitch-angle scattering frequency, we concentrate on the particular region $1-\mu^2 \lesssim \epsilon$. For this, we evaluate the series in Equation (5) for $y \ll 1$. It is clear that the main contribution comes from $n = 1$, but since we also need the sum for $y \sim 1$, we should include a few subsequent terms and examine whether it will change the result substantially. Based on the above remarks about the dominant contribution of the low n terms, it will hopefully not. First, we evaluate S_1 by integrating it by parts and rearranging the remaining integrals as follows:

$$S_1 = \frac{y^{1-q}}{q-3}J_1^2(y) - \frac{2}{q-3}\left(\int_0^\infty J_1(x)J_2(x)x^{1-q}dx - \int_0^y J_1(x)J_2(x)x^{1-q}dx\right). \quad (9)$$

Note that the first term diverges as $y \to 0$, the second is finite, and the third one is small. Neglecting the third term, we obtain

$$S_1 \simeq \frac{3}{4} J_1^2(y)\, y^{-10/3} + S_1',$$

where

$$S_1' = -\frac{567}{6400 \times 2^{1/3}} \frac{\Gamma^2(1/3)}{\Gamma^3(2/3)} \simeq -0.22.$$

Adding to S_1 the leading terms (constants, for $y \ll 1$) from the first few S_n and substituting the obtained $S(y)$ into Equation (4), we arrive at the following final expression for the scattering coefficient:

$$D_{\mu\mu} = \frac{\pi}{2} \frac{v}{l} (1-\mu^2) \left[\frac{J_1^2(y)}{y^2} + r y^{4/3} \right], \tag{10}$$

where $r \sim 10^{-2}$ and $y = \sqrt{(1-\mu^2)/\epsilon}$. Clearly, we can neglect the small second term in the brackets altogether and switch to the expression given by Equation (8) for $y \gtrsim j_1$, where $j_1 \approx 3.8$ is the first root of J_1. Summarizing this section, the most important part of the scattering coefficient $D_{\mu\mu}(y)$ is its sharp peak near $|\mu| = 1$ where it behaves as $D_{\mu\mu} \propto J_1^2(y)$. As y grows and approaches $y = j_1$, $D_{\mu\mu}/(1-\mu^2)$ falls down to $\sim\delta$ of its peak value at $|\mu| = 1$ and remains approximately constant (Equation (8)). The other peak occurs at $\mu \approx 0$ but it is not important for our purposes.

4. PARTICLE PROPAGATION

Suppose that a source of CRs is within the same magnetic flux tube with the Earth. This source could either be an SNR currently accelerating CRs that gradually escape from the accelerator or it could be due to the CRs that have been accelerated not long ago, or any other region of enhanced CRs. We calculate their propagation to Earth below. Obviously, the degree of CR anisotropy near the source may be significantly higher than that observed at Earth. The propagation problem may be considered to be one dimensional and stationary with only the spatial coordinate z, directed along the flux tube from the source to Earth. However, we bear in mind the finite radius of the flux tube by choosing the most important MHD mode that will scatter particles. In particular, out of the three major MHD modes we select the Alfvén wave (with a dispersion relation $\omega = k_\parallel V_A$) since it has no off-axis group velocity component and strong damping as opposed to the fast and slow MHD waves. Note that in a box geometry, rather than in a thin tube geometry, the other modes are also essential for particle scattering (Yan & Lazarian 2002; Beresnyak et al. 2010). On the other hand, for $\mu \approx 1$ propagation, the shear-Alfvén wave is still the most important mode (Chandran 2000).

As the CR particles are assumed to be scattered by Alfvén waves almost frozen into the local fluid, the particle momentum is conserved and the transport problem is in only two variables: the coordinate z and the pitch angle ϑ (or $\mu \equiv \cos\vartheta$). The characteristic (ϑ-independent) pitch-angle scattering frequency ν_ϑ (typical for μ; not too close to $\mu = 0, \pm 1$, where the pitch-angle diffusion coefficient has sharp peaks) can be deduced from the previous section by unifying Equations (6) and (8) (and omitting some factors that are close to unity):

$$\frac{D_{\mu\mu}}{1-\mu^2} \approx \nu_\vartheta \equiv \frac{v}{l} \left(\delta \ln\left(\frac{1}{\epsilon}\right) + \epsilon^{3/2} \right) /6. \tag{11}$$

The equation for the CR distribution thus reads

$$(u+\mu)\frac{\partial f}{\partial z} = \frac{\partial}{\partial \mu}(1-\mu^2) D(\mu) \frac{\partial f}{\partial \mu}. \tag{12}$$

Here, u is the bulk flow (scattering centers) velocity along z in units of the speed of light, $u \ll 1$, and $\mu = \cos\vartheta$. The coordinate z is normalized to the pitch-angle scattering length $c/\nu_\vartheta \approx v/\nu_\vartheta$, so that $D(\mu) = \nu_\vartheta^{-1} D_{\mu\mu}/(1-\mu^2)$, being normalized to ν_ϑ, is close to unity except for the narrow peaks.

Our purpose is to find a narrow feature (which may be a bump or a hole) on the otherwise almost isotropic angular spectrum $f(\mu)$. Clearly, this feature must be pinned to one of the peaks of $D(\mu)$. This feature will be shown to be weak, and so it can be considered independent of the other possible features of $f(\mu)$ that would be related to the remaining two peaks on the function $D(\mu)$; in other words, we apply a perturbative approach.

Let us consider the particle scattering problem given by Equation (12) in a half-space $z \geqslant 0$ and assume that at $z = 0$ (source) the distribution function is $f(0, \mu) = f_0(\mu)$. Note that f_0 is not quite arbitrary since it also contains particles arriving at the source (i.e., those with $\mu < 0$). A similar problem occurs in the DSA at relativistic shocks (Kirk & Schneider 1987; Kirk & Duffy 1999) and in the problem of ion injection into the DSA (Malkov & Voelk 1995). It is clear that if there are no particle sources at $z = \infty$, then $f(\infty, \mu) = f_\infty = \text{const}$, apart from the dependence of f on the particle momentum as a parameter. It is convenient to subtract f_∞ from f:

$$\Psi(z, \mu, p) = f(z, \mu, p) - f_\infty(p), \tag{13}$$

so that the new function Ψ satisfies the same Equation (12) as f and the following boundary conditions:

$$\Psi = \begin{cases} \phi(\mu) = f_0(\mu) - f_\infty, & z = 0 \\ 0, & z = \infty. \end{cases}$$

It is natural to expand the solution into series of eigenfunctions Ψ_λ:

$$\Psi = \sum_\lambda C_\lambda \Psi_\lambda(\mu)\, e^{-\lambda z} \tag{14}$$

obtained from the following spectral problem:

$$\frac{d}{d\mu}(1-\mu^2) D(\mu) \frac{d\Psi_\lambda}{d\mu} + \lambda (u+\mu) \Psi_\lambda = 0. \tag{15}$$

As is well known (Richardson 1918; see also Kirk & Schneider 1987), there exists a complete set of orthogonal eigenfunctions $\{\Psi_\lambda\}_{\lambda_i=-\infty}^{\lambda_i=\infty}$ with discrete spectrum λ_i having no limiting points other than at $\pm\infty$. Therefore, the expansion coefficients C_λ are

$$C_\lambda = \frac{1}{\|\Psi_\lambda\|^2} \int_{-1}^{1} (u+\mu) \Psi_\lambda(\mu) \phi(\mu)\, d\mu, \tag{16}$$

where $\|\Psi_\lambda\|$ denotes the norm of Ψ_λ. Clearly, $\phi(\mu)$ must satisfy the set of conditions $C_\lambda = 0$ for all $\lambda \leqslant 0$. This reflects the fact that ϕ is not an arbitrary boundary condition, as we already noted. Nevertheless, since particles predominantly propagate into the positive z-direction (away from the source), it is reasonable to assume that $\phi(\mu > 0)$ is larger than $\phi(\mu < 0)$, i.e., the source creates the anisotropy. As usual, if we consider the formal solution given by Equation (14) at such a distance z where $(\lambda_2 - \lambda_1) z \gtrsim 1$, with λ_1 and λ_2 being the first (smallest) positive eigenvalues, the solution will be dominated by the first

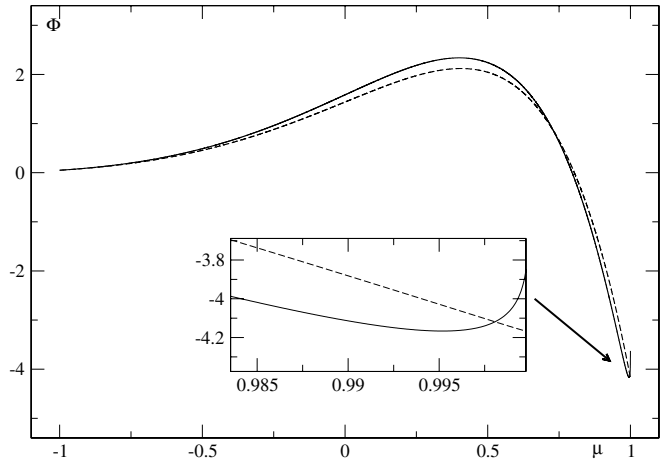

Figure 2. Unperturbed eigenfunction $\Phi(\mu) \equiv \Psi^{(0)}_{\lambda_1}$ (numerical solution of Equation (17); dashed line). Perturbed solution (Equations (19) and (23); solid line). The inset shows the behavior of the solution at the end point, including the logarithmic term of the outer solution.

eigenfunction Ψ_{λ_1}. We know that the anisotropy at Earth is very small ($\sim 10^{-3}$) and, assuming that it is not so small at the source, we deduce that $\lambda_1 z \gg 1$ so that the inequality $(\lambda_2 - \lambda_1)\, z \gg 1$ should be satisfied as well and we can limit our treatment of the spectral problem given by Equation (15) to the determination of only the first positive eigenvalue with the corresponding eigenfunction. We return to this point in Section 5. We also note that since $u \ll 1$, we can set $u = 0$ as there is no significant influence of the region $|\mu| \ll 1$ where Equation (17) has a turning point, whereas we are primarily interested in the behavior of the solution near a singular point at $\mu = 1$. Although the function $D(\mu)$ has a strong peak at $\mu \approx 1$, this peak is very narrow ($\sim\epsilon$) and, as we mentioned, a perturbation theory applies. We start with the outer solution, i.e., with the solution outside of the peak area.

4.1. Angular Distribution Outside the Peak of the Pitch-angle Diffusion Coefficient

Outside the peak region (outer expansion), we assume $D = 1$ as an exact value for D. Therefore, for $(1 - \mu^2) \gtrsim \epsilon$, the zeroth-order approximation reads

$$\frac{d}{d\mu}(1-\mu^2)\frac{d\Psi^{(0)}_\lambda}{d\mu} + \lambda^{(0)}\mu\Psi^{(0)}_\lambda = 0. \tag{17}$$

To find $\lambda^{(0)}$ we require the solution to be regular at both singular points $\mu = \pm 1$. The solution of this problem can be found by a number of numerical methods, for example, by decomposing $\Psi^{(0)}_\lambda$ into a series of Legendre polynomials (e.g., Kirk & Schneider 1987 and references therein). Since we have set $u = 0$ (as opposed to the cited paper where $u \simeq 1$), as few as the first six polynomials would suffice, with a cubic equation for λ. However, Equation (17) contains no parameters (except λ, of course) so that the most practical approach is to find the required single eigenvalue λ_1 and the corresponding eigenfunction by a direct numerical integration of the above equation. The result is shown in Figure 2 and $\lambda_1 \approx 14.54$. Since $\lambda_2 \simeq 2\lambda_1$, the Wentzel–Kramers–Brillouin approximation can be applied for all $\lambda \geqslant \lambda_2$ points of the spectrum. However, the first eigenfunction and the eigenvalue λ_1 is sufficient for our purposes.

Since $D \equiv 1$ in the outer region, the perturbation can be associated only with the perturbation of λ. Therefore, we expand λ and Ψ_λ as

$$\lambda = \lambda^{(0)} + \delta\lambda + \cdots \tag{18}$$

$$\Psi_\lambda = \Psi^{(0)}_\lambda + \delta\lambda\Psi^{(1)}_\lambda + \cdots. \tag{19}$$

Here, λ can be an arbitrary point of the spectrum $\lambda = \lambda_i > 0$, but we are primarily interested in the case $\lambda = \lambda_1$. The equation for $\Psi^{(1)}_\lambda$ takes the following form:

$$\frac{d}{d\mu}(1-\mu^2)\frac{d\Psi^{(1)}_\lambda}{d\mu} + \lambda^{(0)}\mu\Psi^{(1)}_\lambda = -\mu\Psi^{(0)}_\lambda. \tag{20}$$

Since the right-hand side of this equation is not orthogonal to the solution of its homogeneous part (Equation (17)), the operator on the left-hand side of Equation (20) is not identical to the operator in Equation (17). Namely, the regularity condition at $|\mu| = 1$ no longer applies. Instead, a singular, linearly independent counterpart of the solution of Equation (17) should be included (which is appropriate for the outer solution, but not for the inner solution that will be considered in the following subsection). Note that while we are interested in the behavior of the overall solution near $\mu = 1$, we can still require the solution to be regular at $\mu = -1$, since the unperturbed eigenfunction is small there (e.g., Figure 2) and the perturbation at $\mu \simeq -1$ does not significantly influence the overall behavior of the solution. With this in mind, we can write the solution of the last equation as follows:

$$\Psi^{(1)}_\lambda = -\Phi\int_{-1}^{\mu}\frac{U(\mu')d\mu'}{\Phi^2(\mu')(1-\mu'^2)}, \tag{21}$$

where we have denoted $\Phi(\mu) \equiv \Psi^{(0)}_\lambda(\mu)$, and

$$U(\mu) \equiv \int_{-1}^{\mu}\mu'\Phi^2(\mu')d\mu', \tag{22}$$

for short. Two further remarks are in order here. First, the above solution diverges logarithmically when $\mu \to 1$. But, it is not applicable within $1 - \mu \lesssim \epsilon$, where an inner expansion should be obtained and matched to the solution given by the outer expansion (Equations (19) and (21)). Second, the integral in Equation (21) is improper because $\Phi(\mu)$ has zeros, in particular the one at $\mu = \mu_1 \simeq 0.8$ for $\lambda = \lambda_1$. The integral should be understood in terms of a principal value and the solution behaves at $\mu \approx \mu_1$ as $\Psi^{(1)}_{\lambda_1} \propto (\mu - \mu_1)\ln|\mu - \mu_1|$. Before we turn to the inner part of the solution, for the purpose of matching, it is convenient to rewrite the outer solution, given by Equation (21), in the following form:

$$\Psi^{(1)}_\lambda = \frac{U(1)}{2\Phi^2(1)}\Phi(\mu)\ln\left(\frac{1-\mu}{2}\right) - \Phi(\mu) \times \int_{-1}^{\mu}\frac{d\mu'}{1-\mu'}\left[\frac{U(\mu')}{(1+\mu')\Phi^2(\mu')} - \frac{U(1)}{2\Phi^2(1)}\right]. \tag{23}$$

Here, the first term is singular at $\mu = 1$ while the second term is regular there.

4.2. Angular Distribution of the Beam

Turning to the inner expansion of the solution of Equation (15), it is convenient to stretch the variable μ at $\mu = 1$ as follows:

$$w = \frac{1-\mu}{b}. \tag{24}$$

Note that $b = \epsilon j_1^2/2$ is chosen in such a way that $D(w=1) \approx 1$ (see Section 3). Therefore, we represent D as

$$D(w) = \begin{cases} a^{-1}F(w)+1, & w \leqslant 1 \\ 1, & w > 1, \end{cases} \tag{25}$$

with

$$F(w) = \frac{\pi}{2}\frac{1}{j_1^2 w} J_1^2(j_1\sqrt{w}), \quad w \leqslant 1, \tag{26}$$

and $F \equiv 0$ for $w > 1$. Note that $a = \nu_\vartheta l/v \ll 1$ (Section 3). Equation (15) can be written as follows:

$$\frac{d}{dw}[F(w)+a](2-bw)\, w\frac{d\Psi_\lambda^i}{dw} + ba\lambda(1-bw)\Psi_\lambda^i = 0, \tag{27}$$

where the index i stands for the "inner" solution. In contrast to the outer problem, we must impose the regularity condition at $\mu = 1$ ($w = 0$). Since F vanishes for $w > 1$, the expansion of the solution of this equation should be sought in a series of powers of b, not ba, as an inspection of the second term of the equation may suggest. The latter form of the expansion would be valid only for $w < 1$, whereas we need to match the solution of Equation (27) with the outer solution at $w \gtrsim 1$. While the regularity condition at $w = 0$ fixes one of the two arbitrary constants of the solution, it is convenient to choose the second constant as the value of the solution at $w = 0$, i.e., $\Psi_\lambda^i(0)$.

Working up to the second order in $b \ll 1$, and integrating Equation (27) by parts, we transform it into the following first-order equation:

$$\frac{d\Psi_\lambda^i}{dw} + \frac{\lambda b}{2}g'\left[1 - \frac{\lambda b}{2}\left(\frac{h}{w} - g\right)\right]\Psi_\lambda^i = 0,$$

with the following obvious solution:

$$\Psi_\lambda^i(w) = \Psi_\lambda^i(0)\exp\left\{-\frac{\lambda b}{2}g\left(1+\frac{\lambda b}{4}g\right) + \frac{\lambda^2 b^2}{4}\int_0^w g' h dw/w\right\}, \tag{28}$$

where we have used the notation

$$g(w) = a\int_0^w \frac{dw'}{F(w')+a} \tag{29}$$

and

$$h = \int_0^w g(w')dw'.$$

As it is seen from Equation (25), the function g can be evaluated as follows:

$$g = \begin{cases} \frac{8}{\pi}aw, & w < 1 \\ g_1 + w - 1, & w \geqslant 1, \end{cases} \tag{30}$$

where $g_1 \simeq -\sqrt{2\pi a}/J_0(j_1)$. In order to match the inner solution given by Equation (28) with the outer solution obtained earlier (see Equations (19) and (23)), we need to expand both solutions in powers of w or $1-\mu$ which are valid in an overlap region. This is obviously a region where $1-\mu \ll 1$ (to make a series expansion of the outer solution accurate) and $w > 1$ (to make the inner solution simple, e.g., to use Equation (30) for g). As $w = (1-\mu)/b$ with $b \ll 1$, the overlap region exists. Let us write the outer solution given by Equations (19) and (23) in terms of the inner variable

$$\Psi_\lambda = \Phi(1) - \Phi'(1)bw + \frac{1}{2}\Phi''(1)b^2w^2 + \frac{U(1)}{2\Phi(1)}\delta\lambda(\ln w + \ln b) + \mathcal{O}(\delta\lambda + b^3), \tag{31}$$

where the primes denote the derivatives of $\Phi(\mu)$ at $\mu = 1$. The first three terms of the last expression are nothing but the leading terms of the Frobenius expansion of the unperturbed regular part of the solution of Equation (17) at the singular end point $\mu = 1$. The fourth term is a perturbative, singular part of the expansion, which is entirely due to the fact that the spectral parameter λ deviates from its eigenvalue, i.e., $\delta\lambda = \lambda - \lambda_i \neq 0$. Both expansions are written in terms of the inner variable $w > 1$, and thus $D(\mu) = 1$ in Equation (15).

The inner solution given by Equation (28) can be written for $w > 1$ as follows:

$$\Psi_\lambda^i = \Psi_\lambda^i(0)\left[1 - \frac{1}{2}\lambda b(g_1 + w - 1) + \frac{1}{8}\lambda^2 b^2\left(\frac{1}{2}w^2 - 2w + \ln w\right)\right]. \tag{32}$$

Comparing the last two results, we deduce

$$\Psi_\lambda^i(0) \approx \frac{\Phi(1)}{1+\lambda b/2} \tag{33}$$

and

$$\delta\lambda = \frac{\lambda^2\Phi^2(1)}{4U(1)}b^2. \tag{34}$$

Using the matching procedure, we determined the initially unknown arbitrary constant of the inner solution $\Psi_\lambda^i(0)$ and the perturbation of the eigenvalue λ by matching the terms in both equations that are independent of w and proportional to $\ln w$, respectively. The linear and quadratic terms in w automatically match to the appropriate accuracy $\sim b^2$. This follows from the two further relations

$$\Phi'(1) = \frac{\lambda}{2}\Phi(1), \quad \Phi''(1) = \frac{\lambda}{4}\Phi'(1),$$

which can be obtained from the Frobenius series of Equation (17) at the singular end point $\mu = 1$ with $\Psi_\lambda^{(0)} \equiv \Phi$.

The following two observations are important for the goal of this paper. First, since $U(1)$ in Equation (22) is positive definite (which may be readily seen from the equation for Φ, Equation (17), by multiplying it by Φ and integrating by parts), $\delta\lambda$ in Equation (34) is positive definite as well. Of course, this property of the spectrum can be seen directly from Equation (15) by virtue of the positive sign of the perturbation of the coefficient D. Second, the perturbed absolute value of the eigenfunction at $\mu = 1$, given by Equation (33), is always less than the unperturbed one, i.e., $|\Psi_\lambda^i(0)| < |\Phi(1)|$. Below, we discuss the observational consequences of these results.

4.3. Observational Appearance of the Beam

After we have determined the angular distribution of the beam, the question is whether it is consistent with at least the prominent MILAGRO hot spot A (Abdo et al. 2008). There are two observationally testable properties of the solution. The first

property is that the sign of the perturbative correction to the distribution function is opposite, according to Equations (32) and (33), to the sign of $\Phi(1)$. Of course, the latter can be changed arbitrarily but then the main expansion coefficient, Equations (14) and (16), will change its sign as well. Let us fix $\Phi(1) \equiv \Psi^{(0)}_{\lambda_1}(1) < 0$ as shown in Figure 2. Then, the perturbative correction will produce a logarithmic peak at $\mu = 1$ if $C_{\lambda_1} > 0$ and a negative logarithmic hole in the opposite case. As can be seen from Equation (16) and Figure 2, the requirement $C_{\lambda_1} > 0$ constrains the initial distribution $f_0(\mu)$ as follows. While being enhanced in the region $\mu > 0$ (particles propagate predominantly away from the source toward Earth), $f_0(\mu)$ should not be concentrated too close to $\mu \approx 1$. One simple conclusion from this observation is that if an accelerator at $z = 0$ produces a beam of leaking particles, this beam should not be collimated tightly at $\mu = 1$, or even overpopulate the region $\mu_1 < \mu < 1$, where $\Phi(\mu_1) = 0$ with $\mu_1 \simeq 0.8$.

The second property of the solution is that the bump on the particle angular distribution is located at the local minimum of the unperturbed eigenfunction. This is formally not consistent with the MILAGRO results. In contrast, the latter indicates that the bump is in the region of monotonic change of the distribution function. However, the particle distribution obtained above is coming only from the flux tube that connects Earth with the source of the beam. Therefore, to obtain the total distribution, the CR background anisotropic component should be added. The latter, being independent of the beam source, is most likely to change monotonically in any randomly selected area, such as the MILAGRO hot spot A, so there is no apparent contradiction in this regard.

In Section 4.2, the two major beam parameters were calculated in terms of the small parameter of the theory,

$$\epsilon = \frac{r_g(p)}{l},$$

where r_g is the particle gyroradius and l is the maximum wavelength beyond which particles interact with waves adiabatically. The first parameter of the beam is its angular width (in terms of $\mu = \cos\vartheta$)

$$b = \frac{j_1^2}{2}\epsilon \approx 7.3\epsilon \tag{35}$$

and the second is its strength, which can be conveniently expressed as the ratio of the beam excess to the amplitude of the first eigenfunction (Equation (33)):

$$\frac{\delta\Phi(1)}{\Phi(1)} \approx \frac{1}{2}\lambda_1 b \approx 53.4\epsilon\,. \tag{36}$$

Since $\epsilon \propto p$, the spectrum of the beam should be one power harder than the CR large-scale anisotropic component inside the flux tube. This is consistent with the MILAGRO beam spectrum, provided that Φ scales with momentum similarly with the galactic CR background.

According to the MILAGRO Region A observations, the beamwidth is about $\Delta\vartheta \sim 10^\circ$, where $\Delta\vartheta \approx \cos^{-1}(1-b) \approx \sqrt{2b} = j_1\sqrt{\epsilon}$ so that we obtain for ϵ the following constraint from the observed MILAGRO Spot A:

$$\epsilon \approx \left(\frac{\Delta\vartheta}{j_1}\right)^2 \approx 2.1\times 10^{-3}.$$

This estimate yields the strength of the beam given by Equation (36) at the level of ≈0.1 which is also consistent with the MILAGRO fractional excess of the beams A and B measured with respect to the large-scale anisotropy.

In this section, we made a preliminary consistency check of the beam, as it forms while the large-scale anisotropic CR distribution propagates from its source to Earth. In the following section, we verify conditions under which the beam can really reach Earth without self-destruction, as it is well known that beams in plasmas readily become unstable.

4.4. Beam Sustainability

Now that we have calculated the pitch-angle distribution of a narrow CR beam formed from a wide-angle anisotropic CR flux through its interaction with the *background ISM turbulence*, we need to check whether the beam will survive the pitch-angle scattering by *self-generated waves*. The threat is the cyclotron instability of the beam but the hope (as already mentioned by Drury & Aharonian 2008 with regard to the magnetic nozzle) is that the isotropic part of the CR background distribution should stabilize the beam. The dispersion relation is a standard one, which can be written as follows (see, e.g., Achterberg 1983):

$$1 - \frac{\omega^2}{k^2V_A^2} + \frac{4\pi^2e^2}{k}\int \frac{p_\perp^2 dp_\perp dp_\parallel}{p^2(kv_\parallel \pm \omega_c - \omega)} \times\left[p_\perp\frac{\partial F}{\partial p_\parallel} - \left(p_\parallel - \frac{\omega p}{kc}\right)\frac{\partial F}{\partial p_\perp}\right] = 0, \tag{37}$$

where the "±" signs correspond to the left/right polarized Alfvén waves propagating along the field line at the Alfvén speed V_A ($k \approx k_\parallel, \omega \approx \pm kV_A$). The distribution function $F(p_\parallel, p_\perp)$ refers to the sum of the isotropic CR background distribution F_C, the beam distribution F_B, and the large-scale anisotropic part $F_1(p_\parallel, p_\perp)$. The last one, in turn, consists of both the unperturbed solution $\Phi(\mu, p)$, obtained in Section 4.1, and the background large-scale anisotropic component, most likely not related to the source of the beam. Thus, the total distribution function can be represented as $F = F_C(p) + F_B(p_\parallel, p_\perp) + F_1(p_\parallel, p_\perp)$. Since the beam is concentrated at small pitch angles, i.e., $0 < p_\perp \ll p_\parallel$, we assume its contribution to be larger than that of F_1. Clearly, both F_C and F_B are small compared to the background plasma density, which yields the second term in Equation (37).

To simplify the calculations, it is convenient to introduce the new variable ρ instead of using $p_\perp$:

$$\rho = p - \delta p_\parallel \equiv \sqrt{p_\parallel^2 + p_\perp^2} - \delta p_\parallel;$$

here, $\delta = \pm V_A/c$, where the "±" signs relate to the forward and backward propagating waves ($\omega = \pm kV_A$), respectively. Note that the lines of constant ρ coincide with the lines of the quasi-linear diffusion of the distribution function F and with the direction of the differentiation in the brackets in Equation (37). Writing $\omega = \pm kV_A + \gamma$ ($\gamma \ll kV_A$) and neglecting a small term $\delta \ll 1$ in the resonance denominator of Equation (37), we obtain the following relation for the wave growth rate:

$$\gamma = \frac{2\pi^3e^2}{|k|}\delta\int\frac{p_\perp^3}{p}\delta\left(p_\parallel \pm \frac{eB_0}{kc}\right)\left.\frac{\partial F}{\partial p_\parallel}\right|_\rho dp_\perp dp_\parallel.$$

Since $F_C = F_C(p)$ and $\partial F_C/\partial p_\parallel\big|_\rho \approx \delta\partial F_C/\partial p$, the contribution of F_C to the growth rate is stabilizing ($\partial F_C/\partial p < 0$) for both signs of δ and both wave polarizations. The contribution of the beam is destabilizing for both polarizations, as long as the

real part of the frequency is taken as $\omega \approx +kV_A$, i.e., $\delta > 0$. If the beam density were above the instability threshold, it would rapidly spread in pitch angle on the self-generated waves along the lines $\rho = \text{const}$. Therefore, the beam momentum distribution can be obtained from the instability threshold condition, i.e., from an assumption that the imaginary contributions from the beam and from the background CRs cancel. Thus, splitting the total distribution as $F = F_C(p) + F_B(p_\parallel, p_\perp)$ and integrating the terms with F_B by parts in $p_\perp$, we obtain for the growth rate $(0 < \delta \ll 1)$

$$\gamma = \frac{2\pi^3 e^2}{|k|}\delta \int_0^\infty \frac{p_\perp^3}{p^2} dp_\perp dp_\parallel \delta\left(p_\parallel - \frac{eB_0}{|k|\,c}\right) \times \left(2\frac{p_\parallel^2}{p_\perp^2}F_B + \delta p \frac{\partial F_c}{\partial p}\right). \quad (38)$$

The beam contribution to the growth rate suggests the introduction of a beam distribution integrated in $p_\perp$:

$$\mathcal{F}_B(p_\parallel) \equiv \frac{1}{p_\parallel^2}\int p_\perp F_B(p_\perp, p_\parallel) dp_\perp. \quad (39)$$

Note that for the beam particles $p_\parallel \approx p$. Assuming a power-law momentum scaling for $F_C(p) \propto p^{-q_c}$ (with $q_c = 4.6$–4.7, appropriate for the background CR momentum distribution) from Equation (38), we can obtain an expression for the instability threshold distribution $\mathcal{F}_{\rm th}(p_\parallel)$. As we noted, this is the beam distribution that cancels γ in Equation (38):

$$\mathcal{F}_{\rm th}(p_\parallel) \equiv \frac{\delta}{q_c - 2} F_C(p_\parallel), \quad (40)$$

so that if $\mathcal{F}_B(p_\parallel) \leqslant \mathcal{F}_{\rm th}(p_\parallel)$, the beam can sustain its angular distribution. Otherwise, it will spread in pitch angle to satisfy the last inequality. Assuming, however, that this inequality holds, we calculate $\mathcal{F}_B$ using our results from the previous section. First, unlike the threshold function $\mathcal{F}_{\rm th}(p_\parallel)$, which is determined by the isotropic CR background, the momentum dependence of $\mathcal{F}_B(p_\parallel)$ is prescribed by the wide-angle anisotropic component, denoted earlier as $\Phi(\mu)$ (Equations (31)–(33) and (36)). The particle momentum entered this function as a parameter (which we omitted, for brevity) since we were considering only the pitch-angle scattering under the conserved momentum. Using the expressions for the width of the beam and for its amplitude relative to $\Phi(\mu, p)$ given by Equations (35) and (36), respectively, we can represent $\mathcal{F}_B(p_\parallel)$ as follows:

$$\mathcal{F}_B(p_\parallel) = \frac{\lambda_1 b^2}{2} F_0(p_\parallel) = \frac{1}{8}\lambda_1 j_1^4 \epsilon^2 F_0(p_\parallel), \quad (41)$$

where we have denoted $F_0(p) \equiv \Phi(\mu = 1, p)$. Then, our constraint $\mathcal{F}_B(p_\parallel) \leqslant \mathcal{F}_{\rm th}(p_\parallel)$ can be represented in the following way:

$$F_0(p) \leqslant A \frac{V_A}{c}\frac{l^2}{r_g^2(p)} F_C(p), \quad (42)$$

where $r_g = pc/eB_0$ is the particle gyroradius. We denoted by A the following numerical factor:

$$A = \frac{8}{\lambda_1 j_1^4 (q_c - 2)} \approx 10^{-3}.$$

Due to the factor r_g^{-2} in the relation given by Equation (42), the function $F_0(p)$ is constrained at high momenta. Assuming that F_0 is not much steeper than the background distribution F_C, we infer from Equation (42) that there exists a maximum momentum $p_{B\max}$ beyond which the beam would spread in pitch angle and dissolve in the CR background. In fact, we can extract more information from the last constraint. To conform with the MILAGRO results, we assume $F_0 \sim \tilde{F}_C$, where $\tilde{F}_C$ is the anisotropic part of the CR background distribution. It is known to be about $\alpha \sim 10^{-3}$ of the isotropic part F_C, so we can estimate $F_0 \sim \alpha F_C$. The last estimate along with Equation (42) brings us to the maximum beam energy:

$$\frac{p_{B\max}}{mc} \simeq \frac{1}{K}\sqrt{\frac{V_A}{c}\frac{A}{\alpha}}, \quad (43)$$

where we have introduced the following parameter, which is the major small parameter of the theory:

$$K \equiv \frac{c}{l\omega_c} = \epsilon \frac{mc}{p}. \quad (44)$$

Here, ω_c is the proton cyclotron (non-relativistic) frequency and l is the maximum turbulence scale beyond which the particles' response becomes adiabatic. Based on the two independent MILAGRO measurements of the width and the fractional excess of the Beam A, we inferred earlier the parameter $\epsilon \sim 10^{-3}$. Assuming that this value of ϵ relates to the 1 TeV median energy of the MILAGRO collaboration's angular analysis, we obtain for K the value $K \sim 10^{-6}$. Taking $V_A/c \sim 10^{-4}$ and $\alpha \sim A \sim 10^{-3}$, we obtain $p_{B\max} \sim 10$ TeV. This is encouragingly close to the MILAGRO estimates of the beam cutoff energy. We will consider approaches to the independent determination of the theory's small parameter K and the beam's maximum momentum in the following section. Of course, depending on which of the MILAGRO beam measurements (the width, excess, or cutoff momentum) is the most reliable, this quantity may be used to determine K or l.

To conclude this section, we estimate the possible losses of the beam due to the energy-dependent curvature and gradient drifts. Assuming $\nabla \times \mathbf{B} = 0$ and a small propagation angle to the magnetic field (curvature drift dominates), the particle drift velocity can be written as

$$\mathbf{V}_{\rm cd} = \frac{p}{mc}\frac{c^2}{\omega_c B^2}\mathbf{B} \times \nabla B. \quad (45)$$

We can estimate particle displacement across the field line upon traveling a distance of one correlation length l_B as $\Delta r \sim r_g(p) l_B/R$, where R is the typical field curvature. The total displacement from the field line is thus $r \sim r_g\sqrt{L_S l_B}/R \sim r_g\sqrt{L_S/l}$, where L_S is the distance from the source to the observer. The displacement r may be not much larger than the SNR radius, for example, so there should be no significant loss of particle flux due to the drift-related spreading.

5. DISTANCE TO THE SOURCE, BEAM ENERGY WINDOW, AND THE MAXIMUM SCALE l

Assuming only one free parameter $K = c/l\omega_c$ with l being a scale of turbulence (unknown a priori) beyond which particles are not scattered in pitch angle, we have advanced our theoretical construction to the point where it successfully matches the three major MILAGRO observables. These are the angular width of the beam, its excess, and its maximum momentum $p_{B\max}$. Each of those three quantities consistently points to the same value

of $K \sim 10^{-6}$ or $l \sim 1\,\mathrm{pc}/B_{\mu\mathrm{G}}$. In this section, we relate K to two further independent quantities. One of these quantities is the maximum momentum $p_{\max}$ of the CRs accelerated in the SNR which may be responsible for the MILAGRO beam. The other quantity is the distance to this remnant, L_s, or to any other source of energetic particles from which the beam originates. Starting from the source, we represent the decay of the large-scale anisotropic part of the distribution function as follows (see Equations (11), (12), and (14)):

$$F_S(z, p) \sim F_S(0, p) \exp\left[-\mathcal{L}^{-1}\frac{z}{l}\right], \tag{46}$$

where $\mathcal{L}^{-1}(\epsilon)$ is the inverse dimensionless particle scattering length

$$\mathcal{L}^{-1}(\epsilon) = \frac{\lambda_1}{6}\left(\delta \ln\frac{1}{\epsilon} + \epsilon^{3/2}\right)$$

and $F_S(0, p)$ is the anisotropic part of the distribution at the source. As we argued earlier, for the beam to appear at Earth ($z = L_S$) as observed, $F_S(L_S, p)$ should be of the order of the anisotropic part of the local background CRs. Moreover, $\mathcal{L}^{-1}(\epsilon)$ has a minimum ($\approx 1.7 \times 10^{-3}$) at $\epsilon = (2\delta/3)^{2/3} \simeq 1.6 \times 10^{-3}$ for $\delta \equiv V_A/c = 10^{-4}$. This value of ϵ is remarkably close to that inferred earlier from the MILAGRO measurements of the beamwidth and its fractional excess ($\epsilon \simeq 2 \times 10^{-3}$). Since $\epsilon \propto p$, the anisotropic part $F_S(z, p)$ decays rapidly with p. Therefore, for the beam to be observable at 10 TeV, the distance L_s should not significantly exceed the quantity

$$L_{S\max} \approx \frac{6l}{\lambda_1 \epsilon^{3/2}(p_{B\max})} Ln \tag{47}$$

with

$$Ln = \ln\frac{F_s(0, p)}{F_s(L_{S\max}, p)}$$

which can be recast as

$$L_{S\max} \simeq 0.4\frac{c}{\omega_c}\left(\frac{mc}{p_{B\max}}\right)^{3/2} K^{-5/2} Ln$$

or, assuming $K = 10^{-6}$, as inferred from the MILAGRO Spot A parameters, and $B = 3\ \mu$G, we obtain

$$L_{S\max} \simeq 130 \times Ln \times \left(\frac{10\ \mathrm{TeV}}{E_{B\max}}\right)^{3/2} \mathrm{pc}. \tag{48}$$

Given that Ln may be a factor of a few, the last estimate constrains the distance to any SNR, held responsible for the MILAGRO beam, to a few hundreds of parsecs. In fact there is also the lower bound to L_S which, being formally a technical one, may still be meaningful. Indeed, in our calculations of the beam profile, we neglected the contributions of the eigenfunctions corresponding to the eigenvalues λ_n with $n \geqslant 2$. Since $\lambda_2 \simeq 2\lambda_1$, the neglected terms in the spectral expansion of the distribution function would not contribute near $p \sim p_{B\max}$, but they could become essential at lower momenta where $\mathcal{L}^{-1}$ has a minimum as a function of p. That is why we required $\mathcal{L}^{-1}\frac{z}{l} \gtrsim 1$ in Section 4. It does not mean, however, that the beam would not form at these momenta but that its shape may change. Unfortunately, the available MILAGRO data are not sufficient to distinguish between the cases of single and multiple beam eigenfunctions. Nevertheless, the apparent absence of a mesoscale anisotropy (i.e., scales between the narrow beam and the first angular harmonics) hints at the relative unimportance of the higher eigenfunction in the spectral expansion. If this is the case, then the upper bound on L_S given by Equation (48) should be rather close to the lower bound as well.

Let us turn to the question of determining the scale l. The simplest possibility is to associate l with the outer scale of the ISM turbulence. Its typical estimates extend from 1 pc (spiral arms) up to 100 pc for the inter-arm space (Haverkorn et al. 2008). However, a 100 pc scale can hardly be relevant to our analysis for the simple reason that the Larmor radii of the particles of interest are 5 orders of magnitude smaller. Clearly, such long scales should be attributed to the ambient field rather than to the particle scattering field component. On the other hand, as the turbulent energy injected at such long scales cascades to much shorter scales where the wave can interact with 1–10 TeV particles, the spectral energy density is already too low to provide efficient scattering. Clearly, a realistic estimate of the outer scale of turbulence l, relevant to the wave–particle interaction, should be somewhere between these extremes. If particles are propagating from an accelerator, there must be energy injection into the GS cascade at a scale associated with this accelerator. Obviously, l cannot exceed the accelerator (shock) radius. It is interesting to note that the recent optical observations of the SNR 1006 indicate that *ripples* on the shock surface have a scale $\sim$1 pc (Raymond et al. 2007), which is the preferred scale to match the MILAGRO data. From a theoretical standpoint, we need to make an assumption about the accelerator. There are a few possibilities, such as a nearby SNR or a massive blue star surrounded by a wind bubble with the termination shock. Each of these, being magnetically connected with Earth, may accelerate particles and load the connecting flux rope with both the accelerated particles and Alfvénic turbulence. In order to avoid further uncertainties associated with the accelerator, we assume that the turbulence is driven primarily by escaping particles. This is almost certainly the case, once particles escape at a rate sufficient to be detected at Earth. The turbulence, however, may significantly decay along the flux rope due to the relaxation of initially strongly unstable (anisotropic) particle distribution and due to the lateral losses of particles and waves. Note that if these are significant, one should replace $zD(\mu) \to \int Ddz$ in our treatment of particle propagation in Section 4.

The mechanisms of particle escape from an SNR shock, for example, are numerous (Drury et al. 1996; Malkov et al. 2002; Malkov & Diamond 2006; Caprioli et al. 2009; Reville et al. 2009). In almost all cases, the escaping particles are close to the maximum energy achievable in the accelerator and have an anisotropic momentum distribution. Therefore, they should drive Alfvén waves at a scale $l \sim r_g(p_{\max})$. Since $r_g(p) \simeq 10^{-6} B_{\mu\mathrm{G}}^{-1}(p/mc)$ pc, to recover the scale $l \sim 1$ pc, inferred earlier from the beam parameters, it is necessary to assume $E_{\max} \sim 3$ PeV (for $B_{\mu\mathrm{G}} \sim 3$) or precisely the "knee" energy.

6. SUMMARY AND DISCUSSION

The principal results of this paper are as follows. Assuming only a *large-scale* anisotropic distribution of CRs (generated, for example, by a nearby accelerator such as an SNR) and GS cascade of Alfvénic turbulence originating from some scale l, which is the longest scale relevant for wave–particle interactions, we calculated the propagation of the CRs down their gradient along the interstellar magnetic field. It is found

that the CR distribution develops a characteristic angular shape consisting of a large-scale anisotropic part (first eigenfunction of the pitch-angle scattering operator) superposed by a beam, tightly focused in the momentum space in the local field direction. The large-scale anisotropy carries the *momentum dependence* of the source, while both the beam angular width and its fractional excess (with respect to the large-scale anisotropic component) grow with momentum (as $\sqrt{p}$ and p, respectively). Apart from the width and the fractional excess of the beam, the theory predicts its maximum momentum because beyond this momentum the beam destroys itself. All the three quantities are completely determined by the turbulence scale l. Even if l is considered unknown, it can be inferred from any of the three independent MILAGRO measurements. These are the width, the fractional excess, and the maximum energy of the beam, and all three consistently imply the same scale $l \sim 1$ pc. The calculated beam maximum momentum encouragingly agrees with that measured by MILAGRO ($\sim$10 TeV/c). The theoretical value for the angular width of the beam is found to be $\Delta\vartheta \simeq 4\sqrt{\epsilon}$, where $\epsilon = r_g(p)/l \ll 1$. The beam fractional excess related to the large-scale anisotropic part of the CR distribution is $\simeq 50\epsilon$. Both quantities also match the MILAGRO results for $E \sim$ 1–2 TeV. Thus, the beam has a momentum scaling that is one power shallower than the CR carrier it is drawn from. This finding will receive its due discussion.

Obviously, the determination of the absolute value of the beam excess would require the source intensity. Due to the lack of such information, an indirect inference was made in Section 4.3 about the galactic CR (GCR) large-scale anisotropy being of the same order as the large-scale anisotropy responsible for the beam.

Below, the rationale for this admission is given, which we open with the following notations.

1. $\tilde{F}_{\rm GCR}$ and $\bar{F}_{\rm GCR}$ are the large-scale anisotropic and isotropic parts of the galactic (not assumed to be related to the source of the beam) distribution, respectively.
2. $\tilde{F}_S$ and $\bar{F}_S$ (i.e., f_∞ in Section 4) are the similar quantities related to the source of the beam at the distance L_S.
3. F_B is the beam distribution on the top of $\tilde{F}_S$.

Unless the source of the beam is also responsible for the GCR, the quantities $\tilde{F}_S$ and $\tilde{F}_{\rm GCR}$ are independent of each other and cannot be related since the source intensity, the distance to it, L_S, and the losses are unknown. Even if the beam and its carrier $\tilde{F}_S$ propagate without significant losses (or suffer similar losses), the current theory determines only a fractional excess $F_B/\tilde{F}_S \sim 50\epsilon$ (independent of L_S). For the same reasons, we do not know what is the source contribution $\bar{F}_S$ to the total isotropic CR background $\bar{F}_{\rm GCR} + \bar{F}_S$. However, since the beam A is not observed at the minimum[4] of the (measured) total large-scale $\tilde{F}_S + \tilde{F}_{\rm GCR}$ as it would, were $\tilde{F}_S \gg \tilde{F}_{\rm GCR}$ the case (see Figure 2), we infer $\tilde{F}_{\rm GCR} \gtrsim \tilde{F}_S$. Furthermore, since $F_B/\tilde{F}_S$ is calculated and $\tilde{F}_S + \tilde{F}_{\rm GCR}$ is measured along with F_B, both quantities $\tilde{F}_S$ and $\tilde{F}_{\rm GCR}$ can also be determined.

We found that $F_B/\tilde{F}_S \sim 0.1$ for $l \sim 1$ pc which was, in turn, deduced from two other independent measurements (beamwidth $\Delta\vartheta$ and its maximum energy $E_{B\max}$). Since MILAGRO measurements indicate that $F_B/(\tilde{F}_{\rm GCR} + \tilde{F}_S) \sim 0.1$, we conclude that $\tilde{F}_S \sim \tilde{F}_{\rm GCR}$. A more specific relation between the two would not be meaningful since the measurements of $F_B(p)$ are rather limited. If particle losses from the flux tube are negligible, it follows that $\tilde{F}_S(L_S) \sim \tilde{F}_S(0)$ for $p \ll p_{B\max}$ (0 being the source position).

These findings allow us to speculate about the possible source of the beam. First, if the source is an active accelerator that emits strongly anisotropic particle flux, the last relation implies that $\bar{F}_S \sim \tilde{F}_S$. Since by observations $\tilde{F}_S \ll \bar{F}_{\rm GCR}$, such source cannot contribute significantly to the "knee" region at $\simeq$3 PeV. In this case, our inferences of l from three independent measurements—all strikingly pointing at the 3 PeV accelerator cutoff energy (with $l \sim r_g(E_{\max})$)—must be either a coincidence or a different mechanism couples the galactic "knee" particles with the scale of the turbulence that generates the beam. If it is not a coincidence and the source contributes significantly to the observed CR background, the escaping particle flux should be quasi-isotropic, $\tilde{F}_S \ll \bar{F}_S$ (to allow for $\bar{F}_S \sim \bar{F}_{\rm GCR}$). In combination with the assumption that particles escape in the wide range 1 TeV–3 PeV (both to form the beam and to inject MHD energy at the scale l), the source is unlikely to be an active accelerator, but rather a region of enhanced CR density, with a steep cutoff at $\simeq$3 PeV. The near isotropy at the source is not inconsistent with a currently working accelerator, but escape in such a broad energy range probably is inconsistent. Indeed, the available (known to us) mechanisms,which offer a broad energy escape from an SNR along with the spectrum steepening (i.e., spectral break, starting 1–2 orders of magnitude below the cutoff, e.g., Malkov et al. 2005; Malkov & Diamond 2006), at least seem to fall short in covering 3 orders of magnitude in energy. Moreover, for the source to be a recent accelerator (such as a recent SNR, suggested by Erlykin & Wolfendale 1997 with the spectrum E^{-2}) the mechanism should be found that makes the spectrum of the escaping particles at least 0.5 steeper (and steeper still if the acceleration was strongly nonlinear). Combined with the nonlinear acceleration (which is required in the Malkov & Diamond 2006 model) this would make an acceptable spectrum but again it is not clear how these particles can initiate the MHD cascade at such a long scale to ensure the required value of l.

Our argument against the beam and the bulk CR $\tilde{F}_{\rm GCR}$ coming from the same source is that the observed beam is not located at the minimum of the angular distribution of the first eigenfunction, so we need to allow for a second component. This is largely a technical limitation, stemming from the one-dimensional transport model, in which F_B and $\tilde{F}_S$ are coupled, as well as from the single eigenfunction approximation. By removing this latter simplification alone (which is probably even necessary for an accurate description of $\tilde{F}_S$ at TeV energies; Section 5), the above constraint can be relaxed. Another possibility is the lateral diffusion and drifts of the $\tilde{F}_S$ component from the flux tube.

An interesting obvious conjecture from the common origin of the beam and $\tilde{F}_{\rm GCR}$ would be that the proton "knee" at $\simeq$3 PeV is also of the same origin as the beam. However, the beam spectrum is calculated to be one power flatter than its carrier. According to MILAGRO the beam index is about 1.5, so that the carrier should have an index $\simeq$2.5, which is closer to the GCR than to the hypothetical "recent SNR." In particular, this would not support the single-source hypothesis of the GCR "knee" (Erlykin & Wolfendale 1997). Equally problematic would be an

[4] It is interesting to note that Abdo et al. (2008) point out that there is a deep deficit bordering the excess regions. This deficit could be identified as a minimum of the dominant eigenfunction, but they attribute it to the effect of including the excess regions into the background. In other words, the deficit is an artifact of the data analysis.

active accelerator scenario, unless the steepening mechanisms of the runaway CR mentioned above can be adopted after due modifications.

All told, the beam is likely to be at least partly drawn from the GCR (due to the relation between the indices $q_B \simeq q_{\rm GCR} - 1$) but the GS turbulence that creates the beam must be driven by considerably more energetic $\gtrsim$1 PeV particles (due to the constraint $l \simeq r_g$), unless the spiral-arm 1 pc value (Haverkorn et al. 2008) for l is, indeed, acceptable. To explore the possibility of the GCR origin of the beam, an extension of the above model is necessary. At a minimum, the model should include the transport of energetic particles across the flux tube. On the other hand, the particle beaming processes should remain similar to that described in Section 3. However, such consideration is beyond the scope of this paper, particularly because the transport across the flux tube requires a separate study.

Yet another possibility is that the required GS cascade starts in the local interstellar cloud (LIC). It has a suitable size of ~5 pc (Redfield & Linsky 2000) and there would be no problem with the spectrum slope since the beam would be drawn from the GCR with the "right" spectral index $q_{\rm GCR} \simeq 2.7$. Whether the turbulence energy can be injected at the required scale remains to be studied. If it can, the above transport and beam focusing mechanism would be applicable since a parsec wavelength and the GS cascade are the only requirements to draw the beam out of the background CR distribution.

To conclude, the model presented in this paper offers an explanation of the most pronounced MILAGRO beam A, though there are two more beams that need to be explained. One of them is the beam B, ~50° away from beam A, and the second one is in the Cygnus loop area ~100° away. Any attempt to incorporate these two beams into our current model would be speculative. We merely note that the local ISM environment is complicated indeed, thus offering many possibilities in explaining various CR anomalies (e.g., Amenomori et al. 2007). Approaches to the explanation of all three beams based on such a complexity could hardly pass the Occam's razor test. In contrast, the model suggested in this paper is devoid of free parameters, if the knee energy at ~3 PeV can be associated with the maximum CR energy of the source of Beam A. Even though such an association is not proven, our propagation model predicts the following three beam characteristics: its width, fractional excess, and maximum energy are the functions of a single quantity, the longest wave–particle interaction scale l. They all give the correct MILAGRO values for $l \simeq 1$ pc, which is unlikely to be coincidental. However, the exact origin of this particular value remains unclear.

L.O'C.D. and M.A.M. acknowledge the hospitality of KITP in Santa Barbara during the Program Particle Acceleration in Astrophysical Plasmas, 2009 July 26–October 3. The work of P.H.D. and M.A.M. is supported by NASA under the grants NNX 07AG83G and NNX09AT94G and by the Department of Energy, grant DE-FG02-04ER54738.

Note added in proof: During the final editing of this paper we became aware of an alternative explanation of MILAGRO results suggested by Lazarian & Desiati (2010) that will be published in ApJ.

APPENDIX

In this appendix, we provide a sketch of the derivation of the pitch-angle diffusion coefficient $D_{\mu\mu}$ for the anisotropic turbulence of Alfvén waves suggested by Goldreich & Sridhar (1995). We follow a standard line of argument (e.g., Völk 1973). However, we include the finite autocorrelation time as required by the GS spectrum. We start with the equation for the particle momentum **p**:

$$\frac{d\mathbf{p}}{dt} = \Omega \mathbf{p} \times \mathbf{B}/B_0, \tag{A1}$$

where $\Omega = eB_0/p$, $p \gg mc$, and B_0 is the magnitude of the unperturbed magnetic field $\mathbf{B}_0$, assumed to be in the z-direction. We also decompose the total magnetic field **B** in the following standard way:

$$\mathbf{B} = B_0\hat{z} + \sum_{\mathbf{k}} \mathbf{B}_{\mathbf{k}} e^{i\mathbf{kr}}, \tag{A2}$$

where $\hat{z}$ is the unit vector along the z-axis. Note that for the shear Alfvén waves, $\mathbf{B}_{\mathbf{k}} \perp \mathbf{k}, \hat{z}$. As usual, we introduce a spherical coordinate system in the momentum space with the axis along the unperturbed magnetic field: $p_\parallel = p\mu = \mathbf{p}\cdot\hat{z}$, $p_\perp = p\sqrt{1-\mu^2}$, and $p_x + ip_y = p_\perp \exp(i\phi)$. The corresponding notations in **k**-space are $k_\parallel = \mathbf{k}\cdot\hat{z}$, $k_x + ik_y = k_\perp \exp(\alpha_{\mathbf{k}})$, and similarly for $\mathbf{B}_{\mathbf{k}}$: $B_{\mathbf{k},x} + iB_{\mathbf{k},y} = B_{\mathbf{k}} \exp(i\chi_{\mathbf{k}})$, where $\chi_{\mathbf{k}} = \alpha_{\mathbf{k}} \pm \pi/2$, where the "±" sign corresponds to the direction of the wave propagation, $\omega = \pm|k_\parallel|V_A$. With these notations, and also using the relation

$$\mathbf{kr} = k_\parallel v_\parallel t - \xi \sin(\phi - \alpha_{\mathbf{k}}),$$

with $\xi = k_\perp v_\perp/\Omega$, from Equation (A1) we obtain

$$\frac{d\mu}{dt} = \pm\frac{\Omega}{B_0}\sqrt{1-\mu^2}\sum_{\mathbf{k},n} B_{\mathbf{k}} e^{ik_\parallel v_\parallel t + in(\Omega t - \phi_0 + \alpha_{\mathbf{k}})} \frac{n}{\xi} J_n(\xi), \tag{A3}$$

where ϕ_0 comes from the unperturbed particle orbit $\phi = \phi_0 - \Omega t$ and J_n stands for the Bessel function. Denoting by $\Delta\mu$ the variation of μ in time t, for an ensemble-averaged $\langle\Delta\mu^2\rangle$ we obtain

$$\langle\Delta\mu^2\rangle = \Omega^2(1-\mu^2)\sum_{\mathbf{k},n}\int\int_0^t dt'dt'' \times I(k_\parallel, k_\perp, t'-t'') e^{(ik_\parallel v_\parallel + in\Omega)(t'-t'')} \frac{n^2}{\xi^2} J_n^2(\xi),$$

where

$$I_{\mathbf{k}}(t'-t'') = \langle B_{\mathbf{k}}(t')\bar{B}_{\mathbf{k}}(t'')\rangle/B_0^2$$

is assumed to be axially symmetric in **k**-space. Extracting the secular term from the last equation, we obtain Equation (1). Note that it can be further simplified by performing the summation in n:

$$D_{\mu\mu} = -(1-\mu^2)\sum_{\mathbf{k}}\frac{1}{\xi^2}\int_0^\infty I(k_\parallel, k_\perp, \tau) \times e^{ik_\parallel v_\parallel \tau} d\tau \frac{\partial^2}{\partial\tau^2} J_0\left(2\xi\sin\frac{\Omega\tau}{2}\right).$$

REFERENCES

Abdo, A. A., et al. 2008, Phys. Rev. Lett., 101, 221101
Achterberg, A. 1983, A&A, 119, 274
Amenomori, M., et al. 2007, in AIP Conf. Proc. 932, Turbulence and Nonlinear Processes in Astrophysical Plasmas, ed. D. Shaikh & G. P. Zank (Melville, NY: AIP), 283

Bell, A. R. 2004, MNRAS, 353, 550
Beresnyak, A., & Lazarian, A. 2009, ApJ, 702, 1190
Beresnyak, A., Yan, H., & Lazarian, A. 2010, arXiv:1002.2646
Caprioli, D., Blasi, P., & Amato, E. 2009, MNRAS, 396, 2065
Chandran, B. D. G. 2000, Phys. Rev. Lett., 85, 4656
Cho, J., & Vishniac, E. T. 2000, ApJ, 539, 273
Drury, L. O. C., & Aharonian, F. A. 2008, Astropart. Phys., 29, 420
Drury, L. O. C., Duffy, P., & Kirk, J. G. 1996, A&A, 309, 1002
Drury, L. O. C., & Falle, S. A. E. G. 1986, MNRAS, 223, 353
Ellison, D. C., Baring, M. G., & Jones, F. C. 1996, ApJ, 473, 1029
Erlykin, A. D., & Wolfendale, A. W. 1997, J. Phys. G: Nucl. Phys., 23, 979
Goldreich, P., & Sridhar, S. 1995, ApJ, 438, 763
Goldreich, P., & Sridhar, S. 1997, ApJ, 485, 680
Gurevich, A. V. 1961, Sov. J. Exp. Theor. Phys., 12, 904
Haverkorn, M., Brown, J. C., Gaensler, B. M., & McClure-Griffiths, N. M. 2008, ApJ, 680, 362
Jokipii, J. R. 1966, ApJ, 146, 480
Kang, H., Jones, T. W., & Ryu, D. 1992, ApJ, 385, 193
Kennel, C. F., & Engelmann, F. 1966, Phys. Fluids, 9, 2377
Kirk, J. G., & Duffy, P. 1999, J. Phys. G: Nucl. Phys., 25, 163
Kirk, J. G., & Schneider, P. 1987, ApJ, 315, 425
Kruskal, M. D., & Bernstein, I. B. 1964, Phys. Fluids, 7, 407
Lazarian, A., & Desiati, P. 2010, ApJ, in press (arXiv:1008.1981)
Malkov, M. A., & Diamond, P. H. 2006, ApJ, 642, 244
Malkov, M. A., Diamond, P. H., & Jones, T. W. 2002, ApJ, 571, 856
Malkov, M. A., Diamond, P. H., & Sagdeev, R. Z. 2005, ApJ, 624, L37
Malkov, M. A., & Voelk, H. J. 1995, A&A, 300, 605
Maron, J., & Goldreich, P. 2001, ApJ, 554, 1175
Raymond, J. C., Korreck, K. E., Sedlacek, Q. C., Blair, W. P., Ghavamian, P., & Sankrit, R. 2007, ApJ, 659, 1257
Redfield, S., & Linsky, J. L. 2000, ApJ, 534, 825
Reville, B., Kirk, J. G., & Duffy, P. 2009, ApJ, 694, 951
Richardson, R. G. D. 1918, Am. J. Math., 40, 283
Rowlands, J., Shapiro, V. D., & Shevchenko, V. I. 1966, Sov. J. Exp. Theor. Phys., 23, 651
Sagdeev, R. Z., & Shafranov, V. D. 1961, Sov. Phys.—JETP, 12, 130
Salvati, M., & Sacco, B. 2008, A&A, 485, 527
Shapiro, V. D., Quest, K. B., & Okolicsanyi, M. 1998, Geophys. Res. Lett., 25, 845
Sridhar, S., & Goldreich, P. 1994, ApJ, 432, 612
Vedenov, A. A., Velikhov, E. P., & Sagdeev, R. Z. 1962, Nucl. Fusion, Suppl. Part 2, 465
Völk, H. J. 1973, Ap&SS, 25, 471
Yan, H., & Lazarian, A. 2002, Phys. Rev. Lett., 89, B1102
Zank, G. P., Axford, W. I., & McKenzie, J. F. 1990, A&A, 233, 275